Full Paper
doi.org/10.1002/chem.202001544

Cooperative Effects

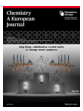

Structural Characterization and Lifetimes of Triple-Stranded Helical Coinage Metal Complexes: Synthesis, Spectroscopy and Quantum Chemical Calculations

Hanna E. Wagner,[b] Patrick Di Martino-Fumo,[a] Pit Boden,[a] Manuel Zimmer,[a] Willem Klopper,*[c] Frank Breher,*[b] and Markus Gerhards*[a]

Abstract: This work reports on a series of polynuclear complexes containing a trinuclear Cu, Ag, or Au core in combination with the *fac*-isomer of the metalloligand $[Ru(pypzH)_3](PF_6)_2$ (pypzH = 3-(pyridin-2-yl)pyrazole). These (in case of the Ag and Au containing species) newly synthesized compounds of the general formula $[\{Ru(pypz)_3\}_2M_3](PF_6)$ (**2**: M = Cu; **3**: M = Ag; **4**: M = Au) contain triple-stranded helical structures in which two ruthenium moieties are connected by three N-M-N (M = Cu, Ag, Au) bridges. In order to obtain a detailed description of the structure both in the electronic ground and excited states, extensive spectroscopic and quantum chemical calculations are applied. The equilateral coinage metal core triangle in the electronic ground state of **2**–**4** is distorted in the triplet state. Furthermore, the analyses offer a detailed description of electronic excitations. By using time-resolved IR spectroscopy from the microsecond down to the nanosecond regime, both the vibrational spectra and the lifetime of the lowest lying electronically excited triplet state can be determined. The lifetimes of these almost only non-radiative triplet states of **2**–**4** show an unusual effect in a way that the Au-containing complex **4** has a lifetime which is by more than a factor of five longer than in case of the Cu complex **2**. Thus, the coinage metals have a significant effect on the electronically excited state, which is localized on a pypz ligand coordinated to the Ru atom indicating an unusual cooperative effect between two moieties of the complex.

Introduction

Nowadays, large heterometallic complexes still lack thorough spectroscopic investigation, in comparison to the large number of investigations on mononuclear[1,2] and polynuclear homometallic[3,4–6] complexes. Especially, heterometallic transition metal complexes are extremely demanding regarding high-level spectroscopic experiments, which is one reason there are so few examples found in the literature.[7] The other reason is that the computational capabilities, which are evolving constantly, have been a limiting factor to understand experimental results in the past, especially with respect to calculations of IR spectra of electronically excited states. Here a full multi-spectroscopic analysis, combined with high level theoretical calculations, is applied to a series of pentanuclear complexes containing three coinage metals.

Complexes consisting of nitrogen donor atoms and coinage metals are frequently occurring protagonists in the field of coordination chemistry. These compounds are not only of high interest because of their wide variety of structural motifs, also a lot of studies concerning the possible applications of these materials (including catalysis,[8] medicine[9] and ionic liquids[10]) have already been performed and demonstrate the manifoldness of these compounds.[11] The heteroaromatic ligand 3-(pyridin-2-yl)pyrazole (pypzH) comprises three *N*-donor atoms and, thus, offers the opportunity of combining several metal atoms in one complex. This ligand can be related to the popular 2,2′-bipyridine ligand (bipy), where tris(bipyridine)ruthenium(II) is probably the most famous representative of its metal complexes.[12] Owing to the additional nitrogen donor, 3-(pyridin-2-yl)pyrazole combines the possibilities to coordinate a ruthenium atom in the octahedral way and to further coordinate more metal atoms after deprotonation. This strategy is related to the upcoming supramolecular approaches in catalysis in-

[a] P. Di Martino-Fumo, P. Boden, Dr. M. Zimmer, Prof. M. Gerhards
Chemistry Department and Research Center Optimas, TU Kaiserslautern
Erwin-Schrödinger-Straße 52, 67663 Kaiserslautern (Germany)
E-mail: gerhards@chemie.uni-kl.de

[b] H. E. Wagner, Prof. F. Breher
Institute of Inorganic Chemistry, Karlsruhe Institute of
Technology (KIT), Engesserstr. 15, 76131 Karlsruhe (Germany)
E-mail: breher@kit.edu

[c] Prof. W. Klopper
Institute of Physical Chemistry, Karlsruhe Institute of
Technology (KIT), Fritz-Haber-Weg 2, 76131 Karlsruhe (Germany)
E-mail: klopper@kit.edu

Supporting information and the ORCID identification number(s) for the author(s) of this article can be found under:
https://doi.org/10.1002/chem.202001544.

volving organometallic complexes.[13,14] For example, van der Vlugt et al. reported on preorganized dinuclear gold complexes for selective catalysis.[14] The first synthesis and X-ray structural analysis of a triple-stranded helical supramolecular complex between two tris{(3-pyridin-2-yl)pyrazole}ruthenium(II) moieties bridged by three copper(I) atoms was reported by Wong et al.[15] in 1997.

In 2014, an article of Ward et al.[16] resumes the supramolecular complex focusing on its role in the separation of the *fac*- and *mer*-isomers of the ruthenium-containing metalloligand $[Ru(pypzH)_3](PF_6)_2$ (**1**), in that case synthesized as hexafluorophosphate salt. They showed that only the *facial* isomer has the ability to form a triple-stranded copper complex, see Figure 1.

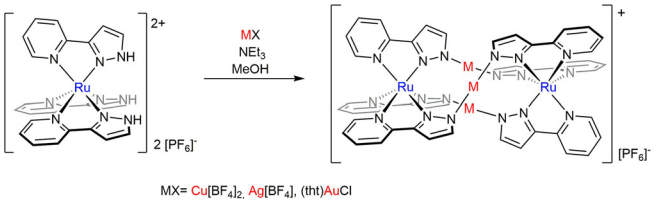

Figure 1. Synthesis of the target compounds **2** (M = Cu), **3** (M = Ag), and **4** (M = Au).

Intrigued by those promising compounds, we decided to further investigate the reactivity of the ruthenium-based metalloligand (**1**) towards the other coinage metals. Due to the close spatial proximity of the three metal atoms incorporated between the two ruthenium(II)-centered ligands, interesting redox and photochemical properties were anticipated. In order to obtain a characterization of the structures both in the electronic ground and excited states, extensive spectroscopic investigations and quantum chemical calculations are required. Alongside X-ray diffraction studies, ^{1}H NMR, UV and especially FTIR spectroscopy as well as time-resolved (step-scan) FTIR (TR-FTIR) spectroscopy were applied to complexes **2**–**4** (Figure 1 and Figure 2). Yielding data of lifetimes in the nanosecond (ns) and microsecond (μs) time-range, the (TR) step-scan FTIR method is especially suited to investigate photophysical and photochemical processes in transition metal complexes,[17] such as photo-activated reactions,[17,18] or excitation and relaxation processes in electronic states.[2,4–6,19–21] In combination with high level quantum chemical calculations, structural changes between different electronic states or different reaction states can be unveiled.

The TR-FTIR investigations have been performed using the sample in its solid form embedded in a KBr-matrix. This technique, presented first by Palmer et al.[20] and established in the Gerhards group,[2,5,6,21] has several advantages for the investigation of transition metal complexes, for example, an extremely large spectral window, the pellets are almost oxygen free (without the need of the pump-freeze technique and the use of inert gas) and can be reused. Furthermore, this technique enables the measurement of complexes that have a poor solubility or dissociate in IR feasible solvents, as KBr is an interference-free matrix.

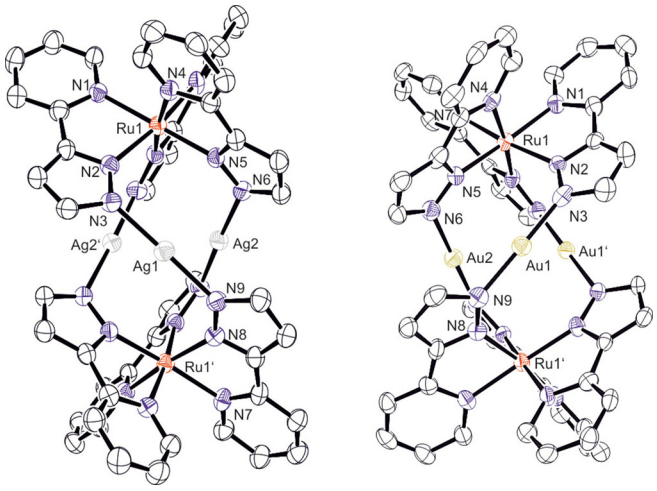

Figure 2. Molecular structures of the silver (**3**, left) and the gold complex (**4**, right). The anion $[PF_6]^-$, solvent molecules and hydrogen atoms have been omitted for clarity, displacement ellipsoids are drawn at the 30% probability level. Selected bond lengths [pm] and angles [°] for **3**: Ru1–N1 207.6(6); Ru1–N2 205.0(6); Ag1–N3 207.0(6); Ag2–N6 207.3(6); Ag1–N9 208.6(6); Ag1···Ag2 323.28; Ag1···Ag1′ 335.32; N3-Ag1-Ag9 176.7(3). For **4**: Ru1–N1 206.1(13); Ru1–N2 204.8(13); Au1–N3 199.6(15); Au2–N6 199.7(16); Au1–N9 194.1(16); Au1···Au2 355.4; Au1···Au1′ 363.6; N3-Au1-N9 178.6(6). See also Table 1.

In addition to the multi-spectroscopic studies, electrochemical investigations were performed by cyclic voltammetry which can be correlated to the UV/Vis data and ionization energies.

Results and Discussion

Crystallography

The already described copper complex crystallizes in the trigonal space group *R*3*c* due to a C_3 rotation axis within the molecule. The silver and the gold complex both crystallize in the monoclinic space group *C*2/*c* with half of the molecule in the asymmetric unit. This reduced symmetry is most likely caused by the residual solvent molecules within the crystal lattices of **3** and **4**. In all three complexes, three (pypz)-M-(pypz) chains connect two Ru^{II} centers to a triple-stranded helix, which are bridged by almost linear N-M-N entities (Figure 2). The crystal structures of all three coinage metal complexes show only minimal differences. The moiety of the ruthenium-based metalloligand of the three different complexes does not reveal any significant differences neither regarding the bond lengths nor the angles between the different atoms. A slight difference can be observed in the distances between the coinage metals embedded in the strands of the helical structure. The gold complex shows the largest interatomic distance of 360 pm whereas the coinage metals in the silver complex seem to be closest (328 pm). With 335 pm (Ø Cu···Cu) the copper complex is comparable with the distances in the silver complex.

This leads to the conclusion that an expected correlation of the distance between the coinage metals and their atom size

cannot be observed. With a Ag···Ag distance of 329 pm the silver atoms in **3** are well within the range (271–365 pm) of proposed argentophilic interactions.[22] The Au···Au distance of Ø360 pm is slightly longer than the distances in complexes where aurophilic interactions (270–350 pm) are discussed.[23] The M–N bonds of all three complexes vary between 185 and 207 pm. The copper complex shows a M–N bond length of 185 pm, whereas the silver complex comprises the longest contact of 207 pm, slightly above the Au–N distances of 200 pm in **4**. Similar compounds in which copper(I) is coordinated by pyrazole moieties also show Cu–N bond lengths of about 185–187 pm.[24,25] Compared to other silver complexes where Ag^+ is coordinated by a pyrazolyl *N*-donor (211 and 225 pm), the Ag–N bond length in **3** is slightly shorter.[24,26] The same statement can be made for the gold complex and similar compounds known from the literature.[27] All three strands connecting the pyrazolyl ligands via a coinage metal center are essentially linear and show angles between 174 and 179 degrees. Most relevant structural parameters are compiled in Table 1. The described crystal structures are in very good agreement with the geometries obtained from FTIR spectroscopy in combination with quantum chemical calculations (cf. FTIR spectroscopy).

Table 1. Selected bond lengths [pm] and angles [°] of **2**, **3**, and **4**.

	Cu (**2**)	Ag (**3**)	Au (**4**)
Ru–N	205	206	205
Ru···Ru	674	706	680
M···M	335	329	360
N–M	185	207	200
N-M-N	175	177	179

UV/Vis spectroscopy and quantum chemical calculations

In the next step, UV/Vis spectroscopy was performed to get a deeper insight into the electronic properties of the complexes. Figure 3 shows the experimental electronic absorption spectra (UV/Vis) of **2**, **3** and **4** in CH_2Cl_2. These spectra were computed (in the gas phase) at the level of TDDFT (cf. section Theoretical Methods).

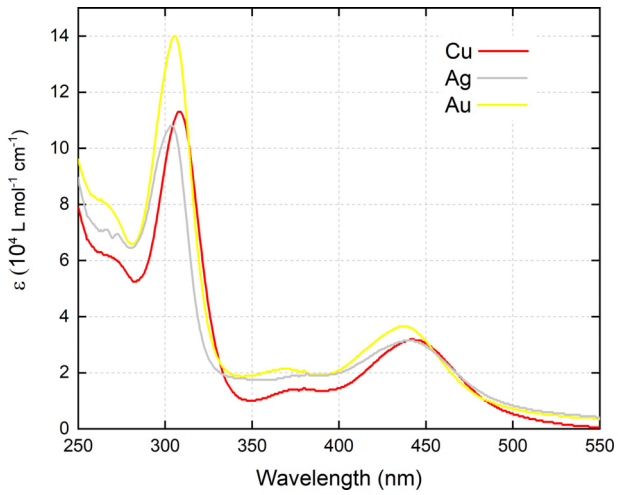

Figure 3. Experimental UV/Vis spectra of **2**, **3** and **4** in CH_2Cl_2.

The TDDFT spectra (Figure 4) compare well with their experimental counterparts (Figure 3). In both the computational and experimental spectra, the bands centered at about 375 and 440 nm are blue-shifted for the Au complex relative to the corresponding bands of the Cu and Ag systems. Similarly, the computations correctly reproduce the experimental observation that the very strong absorption at ca. 300 nm of the Ag complex is blue-shifted with respect to the bands of the Cu and Au complexes.

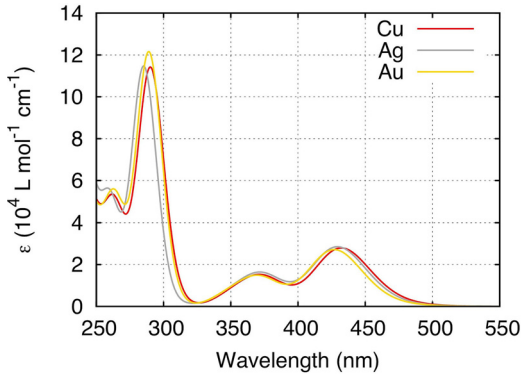

Figure 4. Computed UV/Vis spectra of **2**, **3** and **4**, obtained from TDDFT calculations at the M06/def2-TZVP level (def2-SV(P) for H).

To obtain insight into the UV/Vis spectra, we computed the transition densities for all transitions that contribute to a given band, the underlying transitions being of the same character, respectively. These transition densities were then added (weighted with the oscillator strength of the respective transition) to yield one transition density for visualization of the character of the absorption band.[28]

Figure 5 shows the UV/Vis spectrum of the Cu complex with all underlying transitions (blue sticks) (see Figures SI11 and SI12 for **3** and **4** as well as Table S1). The weighted average transition densities for the bands A through C of Figure 5 are depicted on Figure 6 for **2** (see Figures SI13 and SI14 for **3** and

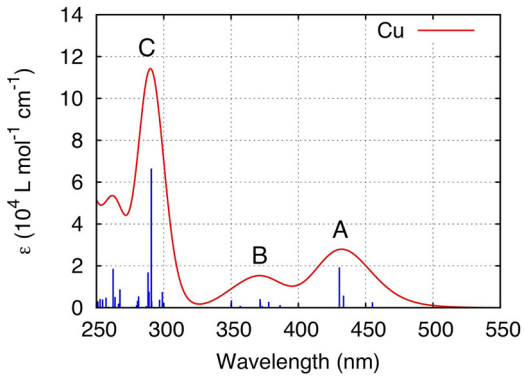

Figure 5. Computed UV/Vis spectrum of **2**, obtained from TDDFT calculations at the M06/def2-TZVP level (def2-SV(P) for H).

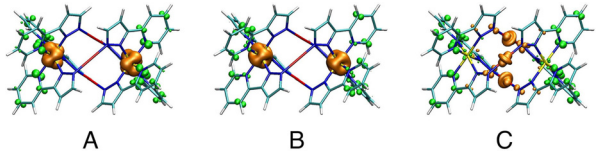

Figure 6. Weighted average transition densities of **2** for the bands A through C of Figure 5. Green corresponds to a gain while orange indicates a loss of electron density (isovalue: $\pm 0.005\ a_0^{-3}$).

4). All excitations with substantial oscillator strength and at wavelengths larger than 325 nm (bands A and B) can be characterized as metal-to-ligand charge-transfer (MLCT) transitions, where electron density is transferred from the Ru centers to the pyridine rings of the ligands (see Table SI1 and Figures SI15, SI16 and SI17). These observations are similar to the behavior of the related benchmark complex $[Ru(bpy)_3](PF_6)_2$ with an intense MLCT absorbance in the visible region (around 450 nm).[29] Just below 300 nm (band C), the main excitation is an MLCT with M being the coinage metal bridge (see Table SI1 and Figures SI15, SI16 and SI17). Electron density is transferred from the coinage metal centers and to a smaller extend the pyrazole units to the pyridine moieties. At this point it should be mentioned that the calculated spectrum of the Ru metalloligand $[Ru(pypzH)_3]^{2+}$ shows a UV/Vis absorbance pattern which is similar to the spectra of the supramolecular complexes, but blue-shifted by about 50 nm (Figures SI18 and SI19). The exchange of the coinage metals does not have a significant influence on orbital shapes, but is responsible for the described small spectral shifts. Further analysis on the electronic properties was performed by cyclic voltammetry (cf. next chapter).

The ground-state structures were optimized in D_3 point-group symmetry for all the complexes. To simulate the experimental step-scan FTIR spectrum, we have also optimized the equilibrium geometry of the lowest lying triplet state and evaluated its harmonic vibrational frequencies (cf. chapter on FTIR and TR-FTIR spectroscopy). The calculations on the triplet state were done in C_1 point-group symmetry, yielding a symmetry-broken solution with all of the spin density located on one of the Ru centers (Figure SI20).

Cyclic voltammetry

Electrochemical investigations were performed in order to further elucidate the influence of the coinage metals on the electronic properties with respect to the Ru^{II}/Ru^{III} redox potential. All complexes undergo two quasi-reversible Ru^{II}/Ru^{III} oxidations (in all cases vs. the Fc/Fc^+ couple, cf. Figure 7). For **2**, the oxidations are observed at $E^0_{1/2} = 0.23$ V and $E^0_{1/2} = 0.12$ V with

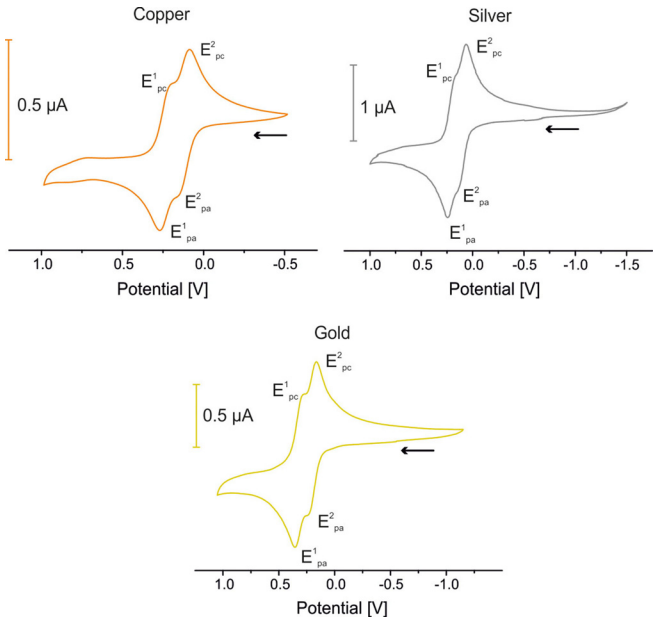

Figure 7. Cyclic voltammograms of **2**, **3** and **4** in CH_2Cl_2. All measurements at room temperature vs. the Fc/Fc+ couple; scan rate $v = 100$ mV s^{-1}, Pt/$[n\text{Bu}_4\text{N}][PF_6]$/Ag.

$\Delta E^0_{1/2} = 110$ mV. Also **3** shows those two quasi-reversible oxidations that appear at $E^0_{1/2} = 0.20$ V and $E^0_{1/2} = 0.11$ V; in this case, the gap is slightly smaller with only $\Delta E^0_{1/2} = 90$ mV. In the gold complex **4**, the potentials of both Ru^{II}/Ru^{III} oxidations are anodically shifted to $E^0_{1/2} = 0.32$ and $E^0_{1/2} = 0.20$ V). Thus, **4** shows the largest difference of $\Delta E^0_{1/2} = 120$ mV between both quasi-reversible oxidations (Figure 7). The small separation between the redox potentials of the two Ru metalloligands indicates that the second oxidation is influenced by the lack of electron density on the other subunit. As the measured $\Delta E^0_{1/2}$ values do not correlate with the spatial distance between the Ru centers (cf. crystallography and calculated geometries) it is suggested that the electronic interaction[30] involves the coinage metal bridges and is not an interaction through space.

The experimental redox potentials $E^0_{1/2}$ were compared with the first and second ionization energies (IE) of **2**, **3** and **4** computed at the G_0W_0 and ev*GW* levels (cf. section Theoretical Methods; see Table 2). At both levels, the 2nd IE is ca. 0.04 eV higher than the 1st IE. The IEs of **3** are 0.01 eV smaller than those of **2**, but the IEs of the gold complex **4** are largest.

Interestingly, the IEs are in very good agreement with the trends observed for the measured $E^0_{1/2}$ values, where the highest redox potential is reached for **4**. This observation also correlates with the effects observed in the UV/Vis spectra as the absorbance bands assigned to transitions of electron density

Table 2. Experimental $E^0_{1/2}$ [V] and $\Delta E^0_{1/2}$ [mV] values and calculated ionization energies [eV] (ev*GW* or G_0W_0/M06/def2-TZVP) of **2**, **3**, and **4**.

	1st $E^0_{1/2}$	2nd $E^0_{1/2}$	$\Delta E^0_{1/2}$	1st IE G_0W_0/ev*GW*	2nd IE G_0W_0/ev*GW*
Cu (**2**)	0.12	0.23	110	7.38/7.56	7.42/7.60
Ag (**3**)	0.11	0.20	90	7.36/7.55	7.41/7.59
Au (**4**)	0.20	0.32	120	7.41/7.58	7.44/7.62

from the Ru centers to the ligands are blue-shifted for complex **4** compared to **2** and **3**. Hence, a higher amount of energy is required to subtract electron density from the Ru centers in the case of **4**.

FTIR and TR-FTIR spectroscopy

FTIR investigations of the electronic ground state of **2**–**4** yield IR spectra showing multiple intense peaks in the region between 1700 and 1300 cm^{-1}. Further, less intense peaks are observed at lower frequencies (Figures 8, SI24, SI27 and SI30).

In order to obtain vibrational assignments, DFT calculations were performed. The experimental ground state FTIR spectra of **2**–**4** are well described by quantum chemical calculations (Figure 9, and Figures SI25, SI28 and SI31), although peak shifts between calculated and experimental frequencies are observed with the calculated ones being lower than the experimental values. It is important to mention that the chosen scaling factor of 0.965 was determined according to the experimental absorption band at 1605 cm^{-1} in the spectrum of **2**. A complete description of the vibrational modes can be found in the Supporting Information (Tables SI2–SI4).

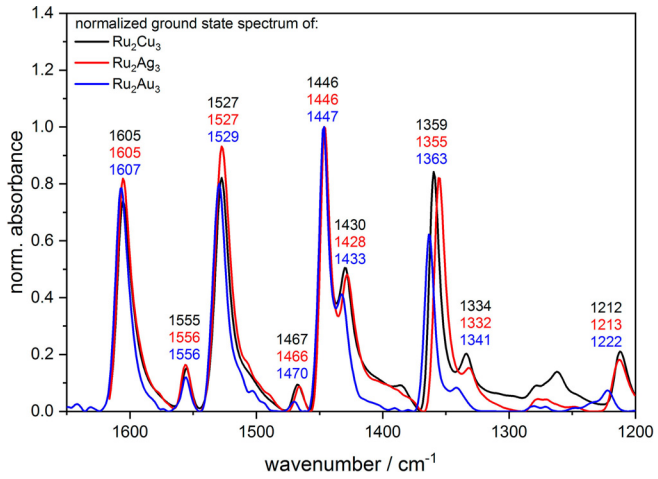

Figure 8. Comparison of the measured FTIR ground state spectra of (**2**) (black), (**3**) (red) and (**4**) (blue).

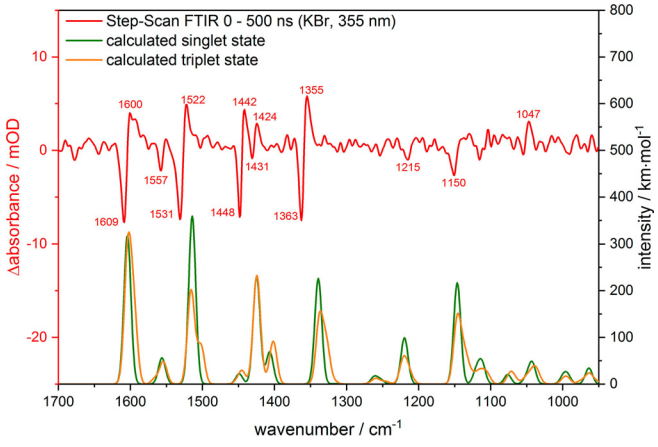

Figure 9. Step-scan FTIR spectrum 0 to 500 ns after irradiation of **2** (red) and calculated IR spectrum of the electronic ground state (green) and excited state (orange) (10 cm^{-1} gauss. convolution). Abscissa of the calculated IR spectra scaled by 0.965. The positive peaks in the transient IR spectrum refer to the electronically excited states whereas the negative ones belong to the electronic ground state.

Step-scan FTIR investigations on **2**–**4** in the time-range between 0 to 500 ns after irradiation with a 355 nm laser pulse result in difference spectra with very sharp and well resolved bands (Figure 9, and Figures SI24, SI27, SI30). The negative peaks indicate the depopulation of the electronic ground state. Positive absorption bands result from vibrations of the populated electronically excited state(s) and are redshifted and lower in intensity compared to the negative bleach bands. This is a general observation for all three complexes. The sharp positive and negative absorption bands can be explained by the comparison of the calculated spectra of the electronic ground and excited states (Figure 9, and Figures SI25, SI28 and SI31). Concerning the excited state calculations, the lowest lying triplet T_1 state was considered for each complex, as the obtained microsecond excited state lifetimes (cf. section Excited state Lifetimes) clearly disagree with the S_1 state and a spin allowed transition from an excited state to the ground state. There are only small differences between the ground state and excited state spectra which is the reason for the observation of very narrow peaks in the difference spectra. The different vibrational frequencies result from the geometry changes after electronic excitation (cf. section quantum chemical calculations). Furthermore, the vibrational transitions calculated for the electronically excited state have lower values than the transitions of the electronic ground state. This is also reflected in the experimental step-scan IR spectrum. As expected from the interpretation based on Figure 9 (here for complex **2**), the overall comparison of experimental and theoretical spectra is very good which is also valid for complexes **3** and **4** (Figures SI28 and SI31).

The infrared spectroscopy allows the investigation of structural differences between **2**–**4**, in the ground state as well as in the electronically excited state. By comparison of the structures obtained from DFT calculations, it is possible to discuss the influence of the coinage metal cations on the helical structure and, thus, their influence on the obtained IR spectra.

The comparison of the D_3-symmetrical singlet states (electronic ground state, Tables 3, SI5, SI7 and SI9) shows that the

Table 3. Selected calculated distances [pm] and angles [°] of **2**, **3** and **4** in the electronic ground state. Level of theory: M06/def2-TZVP, def2-SV(P) for H, def2-ecp for Ru.

		Cu (**2**)	Ag (**3**)	Au (**4**)
S_0	Ru–N_1	210	210	210
	M···M	348	329	354
	A(M_3)–Ru	310	339	327
T_1	Ru–N_{1a}	265	262	262
	M_a···M_b	355	330	348
	M_b···M_c	388	361	386
	M_c···M_a	362	348	378

silver complex contains the smallest coinage metal triangle and the smallest distances among the precious metal cations. The gold complex shows the largest coinage metal-to-metal distances, whereas copper lies in between **3** and **4**. This shows that the structures obtained by combining IR spectroscopy and theory are in a good agreement with the conducted studies of the crystal structures.

In addition, it is notable that the silver complex shows the largest distance between the midpoint of the coinage triangle center and the ruthenium cations, whereby the distance between a silver cation and the Ru center is almost identical to that of the analogue gold complex. Another important aspect is the coordination of the coinage metal cation by the nitrogen atom N_3 of the pyrazoline units (Figure 11). These units contribute significantly to the observed band at ca. 1360 cm^{-1}. This vibration is redshifted for **3** compared to **4**, whereas the frequency of **2** lies in between (Figure 8). The DFT calculations reproduce the relative position of this band correctly for all three complexes (Figure SI34). The influence of the coinage metal, the size of the coinage metal triangle as well as the resulting coordination/overlap of the orbitals with the pyrazole unit can therefore be probed via this band. Indirectly, the octahedral coordination of the ruthenium centers is also influenced, since the coinage metal triangles twist the helical structure.

In the triplet state (electronically excited state) all three structures show very similar tendencies with respect to changes of geometry (Tables 3, SI6, SI8 and SI10). This is mainly due to the occupation of the singly occupied molecular orbital (SOMO) in the excited triplet state, which is of σ^* antibonding character and weakens the N_1-Ru coordination with a significant increase of the corresponding bond length (Figures SI21, SI22 and SI23). The entire system is influenced and, due to the geometric changes, the D_3 symmetry is thereby suspended. The coinage metal triangle is distorted and no longer forms an equilateral triangle. This is clearly visible in the M···M distances and angles as well as in the coordination distances between $N_{2a,b,c}$—Ru. This also has an influence on the band at approx. 1355 cm^{-1} (pyrazole unit). Again, the DFT calculations reproduce the relative positions of this band for each complex as observed in the transient step-scan difference spectra (Figure 10) and in the experimental excited state spectra (Figure SI33), which are generated by addition of a certain percentage of the corresponding ground state spectrum to the step-scan spectrum to suppress the negative bleach bands. It should be noted that only one half of the complex (separation plane is the triangular plane) shows strong changes (Figure 11) and the unaffected side corresponds to the singlet state. The full geometry information of structures obtained from DFT calculations are given in the SI.

These results show that transient step-scan FTIR spectroscopy is a very powerful method to determine even smallest geometrical changes upon electronic excitation of excited states with lifetimes in the nanosecond to microsecond regime (see next paragraph), even for large polynuclear metal containing complexes, which have not been investigated so far by step-scan spectroscopy.

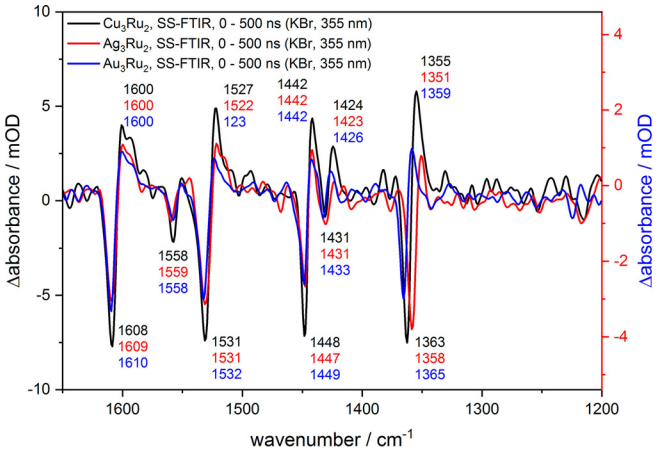

Figure 10. Comparison of the step-scan FTIR difference spectra 0 to 500 ns after irradiation of the complexes **2**–**4** containing Cu, Ag and Au, respectively.

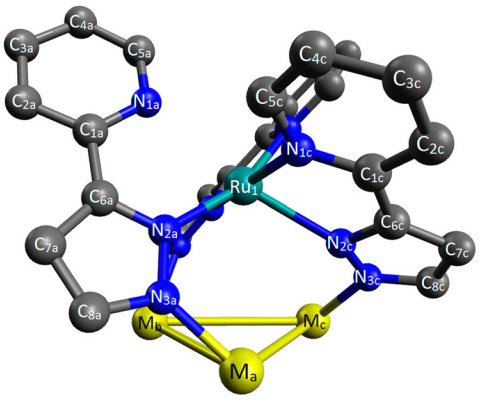

Figure 11. Calculated excited state structure of **2**, showing one half of the complex with one Ru unit (separation plane is the triangular plane), affected by the structural changes with respect to the ground state. Hydrogen atoms have been omitted for clarity.

Excited state lifetimes

In order to obtain the lifetimes of electronically excited states, it turns out that complexes **2**–**4** show an almost vanishing luminescence. Thus, no lifetimes can be obtained by analyzing the luminescence decay times. Substances **2**–**4** are text book examples for a *series* of molecular complexes, which show almost exclusive radiationless decay after electronic excitation. In order to analyze these lifetimes, transient IR spectroscopy offers an ideal tool.

From the step-scan spectra recorded as a function of time delay with respect to the excitation pulse at 355 nm, decay curves were obtained. By performing global fits (Figures SI26, SI29 and SI32) biexponential decay curves are obtained. The first component is in the nanosecond regime and can be attributed to internal conversion processes (see for example, Refs. [5] and [6]). The second most prominent component (about 85 %) is in the microsecond regime resulting in lifetimes of 3.3 µs for **2**, 6.7 µs for **3** and 17.7 µs for **4**. These microsecond lifetimes can be assigned to radiationless decay from the

lowest excited T_1 state to the ground state. The long lifetimes in the microsecond region further confirm the assignment of a triplet state to the step-scan difference spectrum. A very interesting result is the strong dependency of the lifetimes with respect to the coinage metal. At the same time, the calculations predict a charge transfer from one ruthenium center to a coordinating ligand without any contribution of the coinage metals, which are not involved in the S_0 to T_1 transition (Figures SI21, SI22 and SI23). The lifetime of the gold complex **4** is more than five times higher than the corresponding time constant obtained for the copper species **2**. This is a surprising result that may indicate a kind of "inverse" heavy atom effect with respect to the lifetimes of the triplet states. This effect is induced by the coinage metal, which is not implicated into the S_0 to T_1 electronic transition in a direct way. The excited state lifetimes seem to correlate with the changes of the M···M distances upon electronic excitation to the T_1 state (Table 3). In the case of Cu (**2**), all three M···M distances are longer in the excited state compared to the ground state, whereas one M···M gap is unaffected in the case of Ag (**3**) and one M···M distance is even shortened in the excited state of Au (**4**). Smaller distances and thus stronger interactions between the coinage metals in the T_1 state might lead to longer time constants.

The excited state lifetimes are not accessible by luminescence and thus transient IR spectroscopy is an ideal method to analyze these lifetimes and reveal unusual cooperative effects between different parts (coinage metal center vs. ruthenium-based moiety) of the complexes.

Conclusions

In this work, we have described the synthesis as well as the spectroscopic and theoretical characterization of three triple-stranded helical complexes $[\{Ru(pypz)_3\}_2M_3](PF_6)$ (**2**: M = Cu; **3**: M = Ag; **4**: M = Au). The molecular structures were identified by X-ray diffraction, NMR and FTIR spectroscopy. Furthermore, electrochemical measurements and (transient) FTIR spectroscopy on **2**–**4** illustrate the slight but nevertheless important differences between all three compounds. The UV/Vis spectra could be clearly explained by quantum chemical calculations. Time-resolved step-scan FTIR investigations on **2**–**4** in combination with DFT calculations, offer structural changes in the lowest lying electronically excited state (T_1), which was populated by laser excitation. Thus, the influence of the coinage metal centers on the vibrational frequencies was investigated, where small but significant differences were observed. The excited state shows a distortion of the M_3 ring of **2**–**4** leading to a reduction in symmetry and further to changes also in the vibrational frequencies of the ligands. The investigated complexes show no luminescence but from the time-resolved IR spectra, excited state lifetimes could be determined. The excited states (located on a ligand attached to ruthenium) almost only decay radiationless. These lifetimes in the microsecond regime are significantly influenced by the coinage metal leading to an increase by more than a factor of five by going from copper to silver and gold. This interesting "inverse" heavy atom effect could be of interest in future studies and it may also influence (photo)catalytical activities on a reactive center with a second metal center in vicinity but not really involved in the reaction indicating a kind of cooperative effect.

Experimental Section

Experimental setups

All manipulations were carried out with standard Schlenk line and dry-box techniques in a dry argon atmosphere. Methylene chloride and acetonitrile were freshly distilled in an argon atmosphere from calcium hydride. Toluene, diethyl ether and tetrahydrofuran were dried using sodium/benzophenone ketyl. CD_2Cl_2 and CD_3CN were vacuum transferred from calcium hydride into thoroughly dried glassware equipped with Young Teflon valves.

All other reagents were purchased from Aldrich or Roth and used without further purification.

^1H and ^{13}C NMR spectra were recorded with Bruker AV 300 and 400 spectrometers in dry deuterated solvents. The chemical shifts are expressed in parts per millions and ^1H and ^{13}C signals are given relative to TMS. Coupling constants J are given in Hertz as positive values regardless of their real individual signs. The multiplicity of the signals is indicated as s, d, q, sept or m for singlets, doublets, quartets, septets or multiplets, respectively. The assignments were confirmed as necessary with the use of 2D NMR correlation experiments. IR spectra were measured with a Bruker Alpha spectrometer using the attenuated total reflection (ATR) technique on powder samples, and the data are quoted in wavenumbers (cm^{-1}). The intensity of the absorption band is indicated as vw (very weak), w (weak), m (medium), s (strong), vs. (very strong) and br (broad). Melting points were measured with a Thermo Fischer melting point apparatus and are not corrected.

Elemental analyses were carried out in the institutional technical laboratories of the Karlsruhe Institute of Technology (KIT).

Cyclic voltammetry measurements were performed with a suitable potentiostat and an electrochemical cell within a glovebox. We used a freshly polished Pt disk working electrode, a Pt wire as counter electrode, and a Ag wire as (pseudo) reference electrode ($[n Bu_4N][PF_6]$ (0.1 M) as electrolyte). Potentials were calibrated against the Fc/Fc^+ couple (internal standard).

UV/Vis experiments were performed with a Shimadzu UV-1650 UV/vis spectrometer in CH_2Cl_2 solutions (0.002 mM L^{-1}) that were measured in 10 mm path length quartz cells at 20 °C. The spectra were recorded relatively to the pure solvent.

The general experimental setup for step-scan measurements has been described in detail in earlier works,[4–6] so that only a brief description of the general setup is given here.

For the preparation of KBr pellets, compounds **2**–**4** (ca. 2 mg) were mixed with dry KBr (ca. 200 mg, stored in a compartment dryer at 80 °C) and ground to a homogeneous mixture. This mixture was filled into an evacuable pellet die with a diameter of 13 mm and sintered at a pressure of 0.75 GPa. Measurements were conducted under vacuum at room temperature.

All the time-resolved FTIR experiments were performed with the FTIR spectrometer Bruker Vertex 80v, operated in the step-scan mode. A liquid-nitrogen-cooled mercury cadmium telluride (MCT) detector (Kolmar Tech., Model KV100-1-B-7/190) with a rise time of 25 ns, connected to a fast preamplifier and a 14-bit transient recorder board (Spectrum Germany, M3I4142, 400 MS s^{-1}), was used for signal detection and processing.

The laser setup used for the measurements on **2** includes a Q-switched Nd:YAG laser (Lumonics HY 750) generating pulses with a band-width of about 10 ns at a repetition rate of 10 Hz. The setup was modified for **3**–**4** with the implementation of a 100 Hz Nd:YAG laser (Innolas SpitLight Evo I). The third harmonic (355 nm) of the Nd:YAG laser was used directly for sample excitation. The UV pump beam was attenuated to about 3.5 mJ (**2**)/ 2.0 mJ (**3**–**4**) per shot at a diameter of 9 mm. The beam was directed onto the sample and adjusted to have a maximal overlap with the IR beam of the spectrometer. The sample chamber was equipped with anti-reflection-coated germanium filters to prevent the entrance of laser radiation into the detector and interferometer compartments. The temporal resolution of the 14-bit transient recorder board was set to 5 ns. The step-scan measurement was started 2 μs before the laser pulse reached the sample. Hence this time was set as zero point in all spectra. The time delay between the start of the experiment and the laser pulse was controlled with a Stanford Research Systems DG535 delay generator. The spectral region was limited by under-sampling to 0–1975 cm^{-1} or 988–1975 cm^{-1} with a spectral resolution of 4 cm^{-1} resulting in 1110/555 interferogram points, respectively. An IR broad band filter (850–1750 cm^{-1}) and CaF_2 windows (no IR transmission $<1000\ cm^{-1}$) prevented problems when performing a Fourier transformation (i.e., no IR intensity outside the measured region should be observed). FTIR ground state spectra were recorded systematically to check if there is no sample degradation.

Theoretical methods

The TURBOMOLE program package[31] was used for all computations, and the equilibrium geometries (singlet and triplet as ground states) of the complexes were determined at the M06/def2-TZVP [def2-SV(P) for H)][32] level, using def2-ecp pseudopotentials for Ru, Ag and Au.[33]

Vertical transitions were computed (in the gas phase) at the same level of computation. The computed spectra were visualized using Gaussian broadening with a value of 2500 cm^{-1} for the full width at half maximum. The length representation was used for the computation of the oscillator strengths.

The harmonic vibrational frequencies were computed using a shared-memory parallelized version[34] of the AOFORCE module of the TURBOMOLE program package.

G_0W_0 and evGW calculations were performed to obtained quasiparticle energies (IEs) for the HOMO and HOMO-1 orbitals levels. The M06/def2-TZVP orbitals were used and the analytic continuation and contour deformation techniques were applied for G_0W_0 and evGW, respectively.[35]

Synthesis

In order to synthesize the title compounds, both reactions were carried out analogous to the procedures established by Wong and Ward.[15,16] With the aim of obtaining higher yields and easing the purification of the expected complexes, only the pure *fac*-isomer of the ruthenium-containing metalloligand (**1**) was used. The separation of the two isomers was carried out as described by Ward et al. who showed that the pure *fac*-isomer is accessible by reprotonation of the isolated copper complex **2**, as this complex is only formed with this isomer. The pure *fac*-isomer was synthesized as hexafluorophosphate **1**. Upon isolation, we were able to obtain the until now unpublished crystal structure of the pure *fac*-isomer (Figure SI10).

The *fac*-isomer of $[Ru(pypzH)_3](PF_6)_2$ crystallizes in the trigonal spacegroup $P\bar{3}c1$ and the ruthenium center is octahedrally coordinated by the nitrogen chelate ligands. Bond lengths and angles of this metalloligand (Figure SI10) are very similar to the related compound $[Ru(bipy)_3](PF_6)_2$.[36]

Also, the copper intermediate **2** obtained during the isomer separation was synthesized in substantial amounts for further comparison.

The silver complex **3** (Figure 2) was synthesized by the reaction of **1** with an excess of silver tetrafluoroborate in the presence of NEt_3. The reaction mixture immediately turned red and an orange solid precipitated. After purification, **3** was isolated as a red powder in good yields (68%).

The gold complex **4** was obtained with a yield of 64% by similar procedures.

The synthetic procedures are described in more detail in the Supporting Information.

Acknowledgements

Financial support by the Collaborative Research Centre CRC/Transregio 88 "Cooperative effects in homo- and heterometallic complexes (3MET)" is gratefully acknowledged (Projects B4, C1 and C2).

Conflict of interest

The authors declare no conflict of interest.

Keywords: cyclic voltammetry · excited state lifetime · polynuclear complexes · step-scan FTIR spectroscopy · UV/Vis spectroscopy

[1] M. George, *Coord. Chem. Rev.* **1998**, *177*, 201.
[2] S. Treiling, C. Wang, C. Förster, F. Reichenauer, J. Kalmbach, P. Boden, J. P. Harris, L. M. Carrella, E. Rentschler, U. Resch-Genger, C. Reber, M. Seitz, M. Gerhards, K. Heinze, *Angew. Chem. Int. Ed.* **2019**, *58*, 18075; *Angew. Chem.* **2019**, *131*, 18243.
[3] a) A. M. Lunsford, J. H. Blank, S. Moncho, S. C. Haas, S. Muhammad, E. N. Brothers, M. Y. Darensbourg, A. A. Bengali, *Inorg. Chem.* **2016**, *55*, 964; b) D. V. Krupenya, E. O. Danilov, M. A. J. Rodgers, S. P. Tunik, *J. Phys. Chem. A* **2003**, *107*, 8867; c) T. P. Ortiz, J. A. Marshall, L. A. Emmert, J. Yang, W. Choi, A. L. Costello, J. A. Brozik, *Inorg. Chem.* **2004**, *43*, 132; d) J. B. G. Gluyas, A. N. Sobolev, E. G. Moore, P. J. Low, *Organometallics* **2015**, *34*, 3923; e) M. G. Fraser, C. A. Clark, R. Horvath, S. J. Lind, A. G. Blackman, X.-Z. Sun, M. W. George, K. C. Gordon, *Inorg. Chem.* **2011**, *50*, 6093.
[4] M. Zimmer, F. Rupp, P. Singer, F. Walz, F. Breher, W. Klopper, R. Diller, M. Gerhards, *Phys. Chem. Chem. Phys.* **2015**, *17*, 14138.
[5] M. Zimmer, F. Dietrich, D. Volz, S. Bräse, M. Gerhards, *ChemPhysChem* **2017**, *18*, 3023.
[6] F. Bäppler, M. Zimmer, F. Dietrich, M. Grupe, M. Wallesch, D. Volz, S. Bräse, M. Gerhards, R. Diller, *Phys. Chem. Chem. Phys.* **2017**, *19*, 29438.
[7] a) H. Han, Z. Wei, M. C. Barry, J. C. Carozza, M. Alkan, A. Y. Rogachev, A. S. Filatov, A. M. Abakumov, E. V. Dikarev, *Chem. Sci.* **2018**, *9*, 4736; b) J. R. Hickson, S. J. Horsewill, C. Bamforth, J. McGuire, C. Wilson, S. Sproules, J. H. Farnaby, *Dalton Trans.* **2018**, *47*, 10692; c) D. C. Izuogu, T. Yoshida, H. Zhang, G. Cosquer, K. Katoh, S. Ogata, M. Hasegawa, H. Nojiri, M. Damjanović, W. Wernsdorfer, T. Uruga, T. Ina, B. K. Breedlove, M. Yamashita, *Chem. Eur. J.* **2018**, *24*, 9285; d) J. W. L. Wong, S. Demeshko, S. Dechert, F. Meyer, *Inorg. Chem.* **2019**, *58*, 13337; e) R. Horvath, J. Lombard, J.-C. Leprêtre, M.-N. Collomb, A. Deronzier, J. Chauvin, K. C.

Gordon, *Dalton Trans.* **2013**, *42*, 16527; f) A. B. Wragg, S. Derossi, T. L. Easun, M. W. George, X.-Z. Sun, F. Hartl, A. H. Shelton, A. J. H. M. Meijer, M. D. Ward, *Dalton Trans.* **2012**, *41*, 10354.
[8] a) M. M. Díaz-Requejo, P. J. Pérez, *Chem. Rev.* **2008**, *108*, 3379; b) G. J. Hutchings, M. Brust, H. Schmidbaur, *Chem. Soc. Rev.* **2008**, *37*, 1759.
[9] a) I. Ott, *Coord. Chem. Rev.* **2009**, *253*, 1670; b) P. C. A. Bruijnincx, P. J. Sadler, *Curr. Opin. Chem. Biol.* **2008**, *12*, 197.
[10] a) M. Hasan, I. V. Kozhevnikov, M. R. H. Siddiqui, A. Steiner, N. Winterton, *Inorg. Chem.* **1999**, *38*, 5637; b) M. Deetlefs, H. G. Raubenheimer, M. W. Esterhuysen, *Catal. Today* **2002**, *72*, 29.
[11] A. A. Mohamed, *Coord. Chem. Rev.* **2010**, *254*, 1918.
[12] a) P. Dongare, B. D. B. Myron, L. Wang, D. W. Thompson, T. J. Meyer, *Coord. Chem. Rev.* **2017**, *345*, 86; b) K. Kalyanasundaram, *Coord. Chem. Rev.* **1982**, *46*, 159.
[13] a) B. Breit, *Angew. Chem. Int. Ed.* **2005**, *44*, 6816; *Angew. Chem.* **2005**, *117*, 6976; b) Z. J. Wang, K. N. Clary, R. G. Bergman, K. N. Raymond, F. D. Toste, *Nat. Chem.* **2013**, *5*, 100.
[14] V. Vreeken, D. L. J. Broere, A. C. H. Jans, M. Lankelma, J. N. H. Reek, M. A. Siegler, J. I. van der Vlugt, *Angew. Chem. Int. Ed.* **2016**, *55*, 10042; *Angew. Chem.* **2016**, *128*, 10196.
[15] M. H. W. Lam, S. T. C. Cheung, K.-M. Fung, W.-T. Wong, *Inorg. Chem.* **1997**, *36*, 4618.
[16] A. J. Metherell, W. Cullen, A. Stephenson, C. A. Hunter, M. D. Ward, *Dalton Trans.* **2014**, *43*, 71.
[17] G. M. Greetham, D. Sole, I. P. Clark, A. W. Parker, M. R. Pollard, M. Towrie, *Rev. Sci. Instrum.* **2012**, *83*, 103107.
[18] a) J. Torres-Alacan, U. Das, A. C. Filippou, P. Vöhringer, *Angew. Chem. Int. Ed.* **2013**, *52*, 12833; *Angew. Chem.* **2013**, *125*, 13067; b) A. A. Bengali, M. B. Hall, H. Wu, *Organometallics* **2008**, *27*, 5826; c) F. Thibault-Starzyk, E. Seguin, S. Thomas, M. Daturi, H. Arnolds, D. A. King, *Science* **2009**, *324*, 1048; d) J. Torres-Alacan, P. Vöhringer, *Chem. Eur. J.* **2017**, *23*, 6746.
[19] a) P. Chen, R. A. Palmer, *Appl. Spectrosc.* **1997**, *51*, 580; b) D. M. Dattelbaum, R. L. Martin, J. R. Schoonover, T. J. Meyer, *J. Phys. Chem. A* **2004**, *108*, 3518.
[20] G. D. Smith, M. S. Hutson, Y. Lu, M. T. Tierney, M. W. Grinstaff, R. A. Palmer, *Appl. Spectrosc.* **2001**, *55*, 637.
[21] J. M. Busch, D. M. Zink, P. Di Martino-Fumo, F. R. Rehak, P. Boden, S. Steiger, O. Fuhr, M. Nieger, W. Klopper, M. Gerhards, S. Bräse, *Dalton Trans.* **2019**, *48*, 15687.
[22] a) J. C. Garrison, W. J. Youngs, *Chem. Rev.* **2005**, *105*, 3978; b) M. Risto, T. T. Takaluoma, T. Bajorek, R. Oilunkaniemi, R. S. Laitinen, T. Chivers, *Inorg. Chem.* **2009**, *48*, 6271; c) H. Schmidbaur, A. Schier, *Angew. Chem. Int. Ed.* **2015**, *54*, 746; *Angew. Chem.* **2015**, *127*, 756; d) A. Serpe, F. Artizzu, L. Marchiò, M. L. Mercuri, L. Pilia, P. Deplano, *Cryst. Growth Des.* **2011**, *11*, 1278.
[23] a) P. Pyykkö, *Angew. Chem. Int. Ed.* **2004**, *43*, 4412; *Angew. Chem.* **2004**, *116*, 4512; b) A. S. K. Hashmi, I. Braun, P. Nösel, J. Schädlich, M. Wieteck, M. Rudolph, F. Rominger, *Angew. Chem. Int. Ed.* **2012**, *51*, 4456; *Angew. Chem.* **2012**, *124*, 4532; c) H. Schmidbaur, A. Schier, *Chem. Soc. Rev.* **2012**, *41*, 370; d) S. Sculfort, P. Braunstein, *Chem. Soc. Rev.* **2011**, *40*, 2741.
[24] K. Singh, J. R. Long, P. Stavropoulos, *J. Am. Chem. Soc.* **1997**, *119*, 2942.
[25] N. K. Solanki, A. E. H. Wheatley, S. Radojevic, M. McPartlin, M. A. Halcrow, *Dalton Trans.* **1999**, 521.
[26] J. S. Uber, I. Mutikainen, U. Turpeinen, P. Gamez, J. Reedijk, *Inorg. Chem. Commun.* **2007**, *10*, 1478.
[27] R. M. Claramunt, P. Cornago, M. Cano, J. V. Heras, M. L. Gallego, E. Pinilla, M. R. Torres, *Eur. J. Inorg. Chem.* **2003**, 2693.
[28] a) X.-X. Yang, I. Issac, S. Lebedkin, M. Kuhn, F. Weigend, D. Fenske, O. Fuhr, A. Eichhofer, *Chem. Commun.* **2014**, *50*, 11043; b) J. Chmela, M. E. Harding, D. Matioszek, C. E. Anson, F. Breher, W. Klopper, *ChemPhysChem* **2016**, *17*, 37.
[29] N. H. Damrauer, G. Cerullo, A. Yeh, T. R. Boussie, C. V. Shank, J. K. McCusker, *Science* **1997**, *275*, 54.
[30] R. F. Winter, *Organometallics* **2014**, *33*, 4517.
[31] a) TURBOMOLE V7.2 2017, a development of University of Karlsruhe and Forschungszentrum Karlsruhe GmbH, **1989–2007**, TURBOMOLE GmbH, since 2007; available from http://www.turbomole.com; b) F. Furche, R. Ahlrichs, C. Hättig, W. Klopper, M. Sierka, F. Weigend, *WIREs Comput Mol Sci.* **2014**, *4*, 91.
[32] a) Y. Zhao, D. G. Truhlar, *Theor. Chim. Acta* **2008**, *120*, 215; b) F. Weigend, R. Ahlrichs, *Phys. Chem. Chem. Phys.* **2005**, *7*, 3297.
[33] D. Andrae, U. Häußermann, M. Dolg, H. Stoll, H. Preuß, *Theor. Chim. Acta* **1990**, *77*, 123.
[34] C. van Wüllen, *J. Comput. Chem.* **2011**, *32*, 1195.
[35] C. Holzer, W. Klopper, *J. Chem. Phys.* **2019**, *150*, 204116.
[36] Q. Sun, S. Mosquera-Vazquez, L. M. Lawson Daku, L. Guénée, H. A. Goodwin, E. Vauthey, A. Hauser, *J. Am. Chem. Soc.* **2013**, *135*, 13660.

Manuscript received: March 30, 2020
Revised manuscript received: May 12, 2020
Accepted manuscript online: May 19, 2020
Version of record online: July 28, 2020

